

**NASA TECHNICAL
MEMORANDUM**

NASA TM X-52813

NASA TM X-52813

CASE FILE
COPY

**EXPERIMENTAL PERFORMANCE OF A 10 KW,
1200 HERTZ BRAYTON CYCLE ALTERNATOR
AND CONTROLS FOR SPACE POWER**

by Bill D. Ingle and Heinz L. Wimmer
Lewis Research Center
Cleveland, Ohio

TECHNICAL PAPER proposed for presentation at
Fifth Intersociety Energy Conversion Engineering
Conference sponsored by the American Institute
of Aeronautics and Astronautics
Las Vegas, Nevada, September 21-24, 1970

**EXPERIMENTAL PERFORMANCE OF A 10 KW, 1200 HERTZ BRAYTON
CYCLE ALTERNATOR AND CONTROLS FOR SPACE POWER**

by Bill D. Ingle and Heinz L. Wimmer

Lewis Research Center
Cleveland, Ohio

TECHNICAL PAPER proposed for presentation at
Fifth Intersociety Energy Conversion Engineering Conference
sponsored by the American Institute of Aeronautics and Astronautics
Las Vegas, Nevada, September 21-24, 1970

NATIONAL AERONAUTICS AND SPACE ADMINISTRATION

EXPERIMENTAL PERFORMANCE OF A 10 KW, 1200 HERTZ BRAYTON CYCLE
ALTERNATOR AND CONTROLS FOR SPACE POWER

Bill D. Ingle and Heinz L. Wimmer
Lewis Research Center
National Aeronautics and Space Administration
Cleveland, Ohio

Abstract

The performance of the electrical subsystem for a 10-kilowatt 1200-hertz Brayton-cycle power system was experimentally determined. The electrical subsystem under test included the alternator and prototype electronic controls consisting of the voltage regulator and speed control. Both steady-state and transient tests were run under various system-loading conditions. A summary of the test results is presented. In addition, performance criteria and system-interface problems are described.

Introduction

The performance of a voltage regulator and a parasitic speed control on a turbine-driven alternator was determined experimentally. Line voltage and electrical frequency were measured for changes in useful load. Results of the testing are presented for steady-state and transient conditions.

The testing was performed as part of the development program on the 1200 hertz Brayton-cycle space power system (Ref. 1). The alternator in the Brayton system is located on a shaft in common with a turbine and a compressor which operate at 36,000 rpm on gas bearings. For the developmental testing, as reported here, a magnetic equivalent of the alternator which operated on ball bearings was used. This alternator was driven by an air turbine. The electrical control package, which basically consists of a voltage regulator and a parasitic speed control, was fabricated to be capable of operating in a vacuum; however, the testing was performed in air.

Speed control is accomplished by maintaining the input-output power balance of the system. In order to maintain an essentially constant alternator load, the speed controller adjusts the parasitic load as the useful vehicle load is varied. Speed controllers of this type are also used in the SNAP-8 (Ref. 2) and 400 hertz Brayton cycle (Ref. 3) space power systems. The performance characteristics of the individual electrical components, the alternator, the breadboard voltage regulator and speed controller, have been previously reported (Refs. 4, 5). The total test time for all electrical components of this design has exceeded 2000 hours.

The discussion of system performance as included herein presents those characteristics of concern to the potential user of space power generating systems. Therefore the steady-state and transient effects on frequency and load voltage are presented for various loading conditions. Further detailed information on the performance of the specific components is being analyzed.

Test System

A block diagram of the system being tested is illustrated in Fig. 1. The components comprising the test rig are the 1200 hertz alternator operating at 36,000 rpm and the electrical control package (ECP) which basically consists of a voltage regulator, and a parasitic-loading speed controller. The alternator was driven by a commercial air turbine in which the turbine-alternator assembly had an inertia of $0.039 \text{ in-lb-sec}^2$ ($4.5 \times 10^{-3} \text{ kg-m}^2$). The inertia of the turbine-alternator assembly in the test rig has to be considered since it did not match that of the prototype being simulated. The prototype is the Brayton rotating unit (BRU) as used in the Brayton engine (Ref. 1). The inertia of the BRU is $0.058 \text{ in-lb-sec}^2$ ($6.7 \times 10^{-3} \text{ kg-m}^2$).

An analysis was made to investigate the effect of different rotational inertias on the stability of the system. The result is that for increasing inertia the response of the frequency becomes slower and more stable. The higher inertia of the BRU would make the Brayton system more stable than the test rig. Therefore, if the test rig is stable for the same speed control settings, stable operation of the Brayton system will be obtained. The results of this test program did show that the test rig was stable. These electrical control func-

tions utilize all static components and are designed to operate in a vacuum environment. The control package is cooled by attachment to a liquid-cooled cold plate.

A photograph of the test rig is shown in Fig. 2. The alternator is shown at the upper right. Connections for the coolant, bearing lubrication and electric power are visible. The electrical control package (ECP) is shown in the foreground together with the liquid-cooled cold plate. The parasitic and vehicle load banks are not included in this photograph. The useful (vehicle) load rating of the system is 10 kW, 0.85 PF lagging.

The system performance goals are summarized in table I.

Alternator

In Fig. 3, a photograph of the alternator including a schematic cross-sectional view is shown. The photograph illustrates the various connections for coolant, cavity pressurization, bearing lubrication, and electrical power. The alternator as indicated by the cross-sectional view is a modified-Lundell (Rice) design (Refs. 5, 6). The alternator is a solid-rotor, 4-pole machine designed to produce 10.7 kW at 0.75 power factor with a coolant temperature at 70° F . The advantages of this machine are the smooth rotor which minimizes the windage loss and the short armature coils when compared to the homopolar inductor alternator as used in the previous systems. Additional features of this machine are (1) the use of two fields, where one field is excited in proportion to line current and the other field is excited as needed to maintain a constant line voltage; (2) the use of dual heat exchangers to provide redundant cooling paths; and (3) the use of multi-circuit paralleled armature windings to minimize the forces produced by magnetic unbalances. The weight of the alternator is 51 pounds of which the rotor weight is 12 pounds.

Electrical Control Package

In Fig. 4, a photograph of the electrical control package (ECP) including block diagrams of the voltage regulator and speed controller is shown. The right side of the photograph of Fig. 4(a) illustrates the connections for alternator power input, the vehicle power (load) output and various control inputs. The center of the photograph shows the connections to the separately-mounted parasitic load resistor. Adjustments for the voltage regulator and the speed controller are accommodated through openings in the cover. The photograph further illustrates the approximate arrangement of the functional circuits within the control package. The significant feature of the speed controller is that three (3) separate channels are utilized to obtain the desired function. The block diagram of the individual channels is shown in Fig. 4(b). The system improvements obtained with the use of multi-channel speed controllers has been studied separately (Ref. 7). Basically the improvements consist of a reduction in KVA rating on the alternator, and a reduction in the voltage distortion at the vehicle load bus. In this speed control philosophy, the individual channels are tuned such that one channel is essentially full on prior to the start of turn on for the succeeding channel. A desirable effect of this stagger tuning is to generate a more linear control characteristic. The individual channels each consist of a frequency detector, signal amplifiers, and three single-phase, full-wave, phase-controlled power output stages. The system requirements placed special emphasis on minimizing the power losses within the speed controller. The power loss in each channel at minimum parasitic power output is estimated at 21 watts.

In Fig. 4(c), the shunt field regulator block diagram is shown. The regulator operates in a switching mode in which the frequency of operation is synchronized with the alternator line frequency (Refs. 4 and 5). The shunt field regulator includes a current limiting function as required during system startup and during sustained overloads. The free-wheeling diode, D_1 , converts the pulse-width-modulated field voltage to an unidirectional current as required for alternator

excitation. The regulator senses the average value of the peak line voltage. As a result, the value of crest factor for the line voltage has a significant effect on system voltage regulation. In a system having very little line voltage distortion, the effect in voltage regulation is negligible. However, if the distortion increases or varies for any reason, a noticeable effect on system voltage regulation will be apparent. This phenomenon will receive further attention later in the report. The power loss in the shunt field regulator is 41 watts for a vehicle load of 10 kW.

The series field of the alternator is excited in proportion to line current. The series field controller basically consists of current transformers and a bridge rectifier. The losses in the unit at 10 kW vehicle load is estimated at 10 watts. The series field controller in addition to the shunt field regulator comprise the voltage regulator as applied to this electrical control package (ECP).

System Performance

The test data included herein present those system characteristics of immediate concern to the potential user of space power generating systems.

The test data will be presented in two parts. First, the steady-state characteristics of the electrical system are presented as a function of vehicle load. The system parameters being presented here involve the load effects on line frequency and voltage and include photographs of the voltage waveshape. The system loading effects presented here are those generated for vehicle loads having 0.85 PF lagging. Part 2 will present the dynamic characteristics of the electrical system as a function of step vehicle load changes. These characteristics include the load effects on the voltage and frequency as well as the respective recovery times.

Steady-State Characteristics

The control of alternator frequency (speed) as provided by the speed controller is illustrated in Fig. 5. Tests were conducted over a 0 to 10 kWe range of vehicle loads. The vehicle load power factor was 0.85 lagging. As indicated, a 25 hertz control range was obtained over the load range. The 25 hertz control range represents a system speed regulation of approximately 2 percent (2.07). The speed characteristic ideally should be linear with vehicle load. The deviation as evident in Fig. 5 is a function of the speed control design philosophy and the alignment therein. The nonlinearity of the speed control channels is the primary cause for the deviation. The vehicle load voltages are plotted as a function of vehicle load in Fig. 6. The phase voltages ranged from 122.4 volts RMS to 118.0 volts RMS over the load range. This amounts to a voltage change of ± 1.8 percent as compared to the system regulation design goal of ± 1 percent. This variation in phase voltage is a function of the alternator phase balance, the speed control parasitic-power phase balance, and the line voltage distortion. The latter item is the most significant cause of line voltage variation. The distortion of line voltage changes the relation between the RMS value and the peak value. As such the peak-sensing voltage-regulator does not regulate to a constant value of RMS line voltage, which is the parameter, plotted in the figure. Several modifications to the system have been considered to remedy this effect.

This relation between the peak voltage and the RMS value, which is defined as crest factor, is plotted in Fig. 7 as a function of vehicle load. The crest factor varied from 1.47 to 1.24 over the load range in this system. The crest factor was determined from the phase A alternator voltage which is plotted in Fig. 7(b). Nominally the crest factor has a value of $\sqrt{2}$.

The RMS line voltage varied inversely as the crest factor. This relation between crest factor and RMS line voltage would tend to minimize the peak voltage variation at the input to the voltage regulator.

Photographs of the line voltage illustrating the distortion present are shown in Fig. 8. The voltage wave shape at 10 kWe vehicle load had the minimum distortion of any load point. The voltage waveshapes at 1, 5, and 7 kWe vehicle load represent the maximum distortion load points which occurred in the system.

The effect of a change in cold plate temperature on the frequency

and voltage of the system is shown in table II. The load on the system was maintained at 10 kWe, 0.85 PF. A 33° centigrade increase in the cold plate temperature increased the operating frequency by 3.6 hertz, from 1200.2 to 1203.8 hertz. This represents a 0.3 percent change in the system frequency. The line voltage decreased by 0.3 volts from 120.1 to 119.8 volts. This represents a 0.25 percent change in the system voltage.

Dynamic Characteristics

The response of voltage and frequency to a step application of full vehicle load (10 kWe, 0.85 PF lagging) is illustrated in Fig. 9(a) and (b) respectively. The figure indicates that the frequency is overdamped and the frequency (speed) recovery time is approximately 0.19 seconds. The frequency recovery time is defined as the time for the frequency to enter and remain within ± 2 hertz of its final value. The voltage recovery time is defined as the time for the voltage to return to and remain within the 120 ± 6 volt band. The voltage recovery time for this load application is 0.055 seconds. The voltage transient is effectively over in 0.07 seconds. The remaining variations in voltage are a function of the interaction between speed control and the voltage regulator. These voltage fluctuations continued for the duration of the speed transient. The magnitude of the initial voltage transient was approximately 20 volts. This represents an initial undershoot in line voltage to 82 percent of rated.

The response of voltage and frequency to a step removal of full vehicle load is illustrated in Figs. 10(a) and (b), respectively. The figure indicates that the frequency is underdamped and the frequency (speed) recovery time is approximately 0.16 seconds. The voltage recovery time is about 0.074 seconds. The change in voltage and frequency times are a function of the respective control devices. The voltage regulator utilizes field forcing only during the application of vehicle loads. The speed controller utilizes parasitic power forcing only during the removal of vehicle loads (Ref. 5). The voltage transient is effectively over in 0.18 seconds and again the remaining variations are a function of the interaction between speed control and the voltage regulator. The magnitude of the initial voltage transient was approximately 27 volts. This represents an initial overshoot in line voltage to 123 percent of rated. The frequency overshoot was 2 hertz or 0.16 percent of the final value.

The peak value of the line voltage as obtained in the system for a range of step changes in vehicle load are shown in Fig. 11(a). The corresponding recovery times are shown in Fig. 11(b). The largest effect on line voltage occurred for a step change of 10 kW, 0.85 PF lagging vehicle load. The magnitude of the voltage, as previously stated, was 83 percent for load application and 123 percent for load removal. This compares with the system goal of 136 percent of rated maximum. The smallest effect on voltage occurred for a 1 kW, 0.85 PF vehicle load change. The voltage magnitude at this load went to 97.7 percent of rated for load application and 102.6 percent for load removal. The change in the magnitude of the voltage between these two load points was approximately linear. The voltage recovery times for vehicle load changes of 1, 2, and 3 kW at 0.85 PF are zero by definition, since the voltage excursions did not exceed the design goal of 120 volts ± 6 volts. The voltage recovery times for a 9 kW and 10 kW step application in vehicle load are noticeably higher than the remaining recovery times. This occurred because the voltage system is underdamped, and as such, the voltage undershoot exceeded the 6 volt design goal. The maximum voltage recovery time as stated in the system design goals is 0.25 seconds. The recovery times recorded in these tests are well within the system goals.

The magnitude of the frequency (speed) for a range of step changes in vehicle load are shown in Fig. 12(a). The corresponding recovery times are shown in Fig. 12(b). The peak frequencies obtained includes the effect of the steady-state control characteristic, as does all transient test data. With a step application of 7 kW, 0.85 PF vehicle load, the system frequency dropped to 100.8 percent of rated as indicated in Fig. 12(a), and subsequently returned to 101 percent of rated at steady-state as shown in Fig. 5. The highest transient frequency of 102.25 percent occurred for a 9 kW vehicle load change. The lowest transient frequency coincided with the steady-state frequency at 10 kW vehicle load which states an undershoot did not exist for this load application, or the frequency loop was overdamped at this load point. The frequency recovery times, as shown in Fig. 12(b), range from zero to 0.28 seconds for load appli-

cations and from zero to 0.16 seconds for load removal. The frequency recovery times for a step application of 7 and 8 kW, 0.85 PF vehicle load are noticeably higher than the remaining recovery times. This occurred because the system response at those loads was extremely underdamped, and as such, the frequency undershoot exceeded the 2 hertz design goal. The recovery time for a vehicle load change of 1 kW at 0.85 PF was zero by definition, since the frequency excursion did not exceed ± 2 hertz of the final frequency.

The maximum frequency recovery time as stated in the system design goals is 1.0 seconds. The recovery times recorded in these tests are well within these goals.

Concluding Remarks

The results of the test program indicate that the performance of the system was quite satisfactory. No instabilities or significant deviations from system design goals were encountered. The line voltage variation over the 0 to 10 kW, 0.85 PF lagging vehicle load range was ± 1.8 percent, as compared to a system regulation goal of ± 1.0 percent. The crest factor ranged from 1.47 to 1.24 for this load range. This effect is the result of component interaction and system modifications could be made to minimize this effect. No other deviations from the system design goals were encountered. Additional results are itemized below:

1. A frequency control range of 25 hertz (2.07 percent of rated) was obtained over a 0 to 10 kW, 0.85 PF vehicle load range.
2. The peak line frequency was 102.25 percent of rated for a 9 kW step removal of vehicle load and 100 percent of rated for a 10 kW step application of vehicle load. The largest frequency recovery time was 0.28 seconds which occurred for a 8 kW step application of vehicle load.
3. A 33° centigrade change in cold plate temperature resulted in a 0.3 percent (3.6 hertz) increase in operating frequency and a 0.25 percent (0.3 volt) decrease in line voltage.
4. The peak line voltage was 123 percent of rated for a 10 kW step removal of vehicle load and 82 percent of rated for a 10 kW step application of vehicle load. The largest voltage recovery time was 0.074 seconds which occurred for an 8 kW step removal of vehicle load.

TABLE I. SYSTEM PERFORMANCE GOALS

Voltage	
Rated ($=E_R$)	120/208 3 ϕ
Regulation	$\pm 1\%$
Recovery time ($\Delta E \leq \pm 5\% E_R$)	1/4 sec
Maximum transient	^a 136%
Frequency	
Rated ($=F_R$)	1200 hertz
Regulation	$\pm 1\%$
Recovery time ($\Delta F \leq \pm 2$ Hz of F_R^b)	1 sec
Excursion (MAX)	$\pm 2\%$

^aAlternator VR combination only.

^b F_R = final frequency.

References

1. Klann, J. L., "2 to 10 Kilowatt Solar or Radioisotope Brayton Power System," Intersociety Energy Conversion Engineering Conference, Boulder, Colorado, Aug. 14-16, 1968, Vol. 1, IEEE, New York, 1968, pp. 407-415.
2. Nice, A. W. and Bradley, S. L., "SNAP-8 Electrical System," IEEE Transactions on Aerospace, Vol. AS-2, No. 2, Apr. 1964.
3. Word, J. L., Fischer, R. L. E., and Ingle, B. D., "Static Parasitic Speed Controller for Brayton-Cycle Turboalternator," TN D-4176, 1967, NASA, Cleveland, Ohio.
4. Ingle, B. D. and Corcoran, C. S., "Development of a 1200-Hertz Alternator and Controls for Space Power Systems," Intersociety Energy Conversion Engineering Conference, Boulder, Colorado, Aug. 14-16, 1968, Vol. 1, IEEE, New York, 1968, pp. 438-447.
5. Anon.: The 1200-Hertz Brayton Electrical Research Components, "APS-5286-R, NASA CR-72564, Ai Research Mfg. Co., Phoenix, Ariz., Mar. 1969.
6. Repas, D. S. and Edkin, R. A., "Performance Characteristics of a 14.3 Kilovolt-Ampere Modified Lundell Alternator for 1200 Hertz Brayton-Cycle Space-Power System," TN D-5405, 1969, NASA, Cleveland, Ohio.
7. Gilbert, L. J., "Reduction of Apparent-Power Requirement of Phase Controlled Parasitically Loaded Turboalternator by Multiple Parasitic Loads," TN D-4302, 1968, NASA, Cleveland, Ohio.

TABLE II. EFFECT OF TEMPERATURE ON OPERATING FREQUENCY AND VOLTAGE AT 10 kW_e, 0.85 POWER FACTOR, VEHICLE LOAD FOR A TOTAL ALTERNATOR LOAD OF 10.7 kW_e

Temperature of cold plate		Operating frequency	Line voltage (3 ϕ average)
$^{\circ}$ C	$^{\circ}$ F	Hz	V, rms
22	72	1200.2	120.1
30	86	1201.6	119.8
43	109	1202.9	119.9
55	131	1203.8	119.8

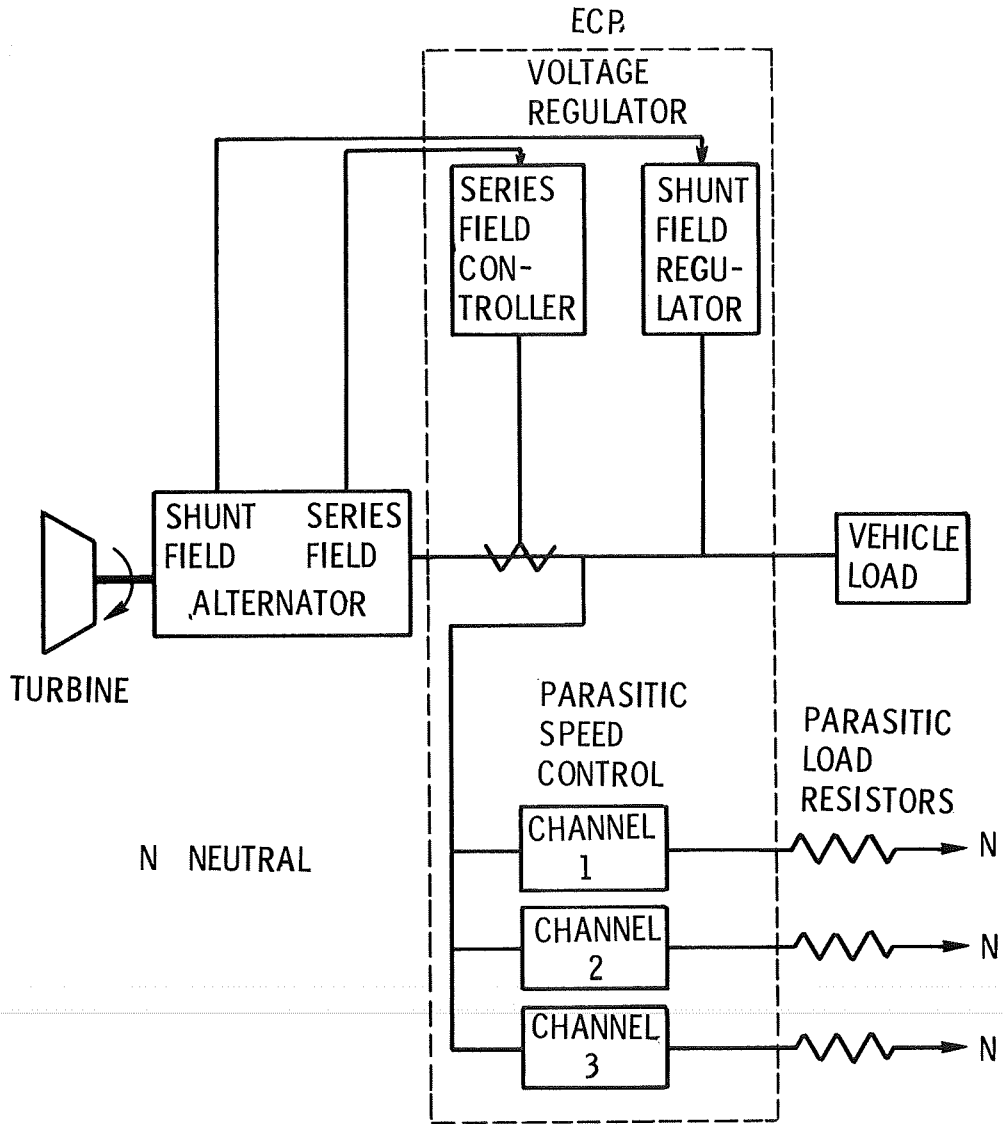


Figure 1. - Electrical system.

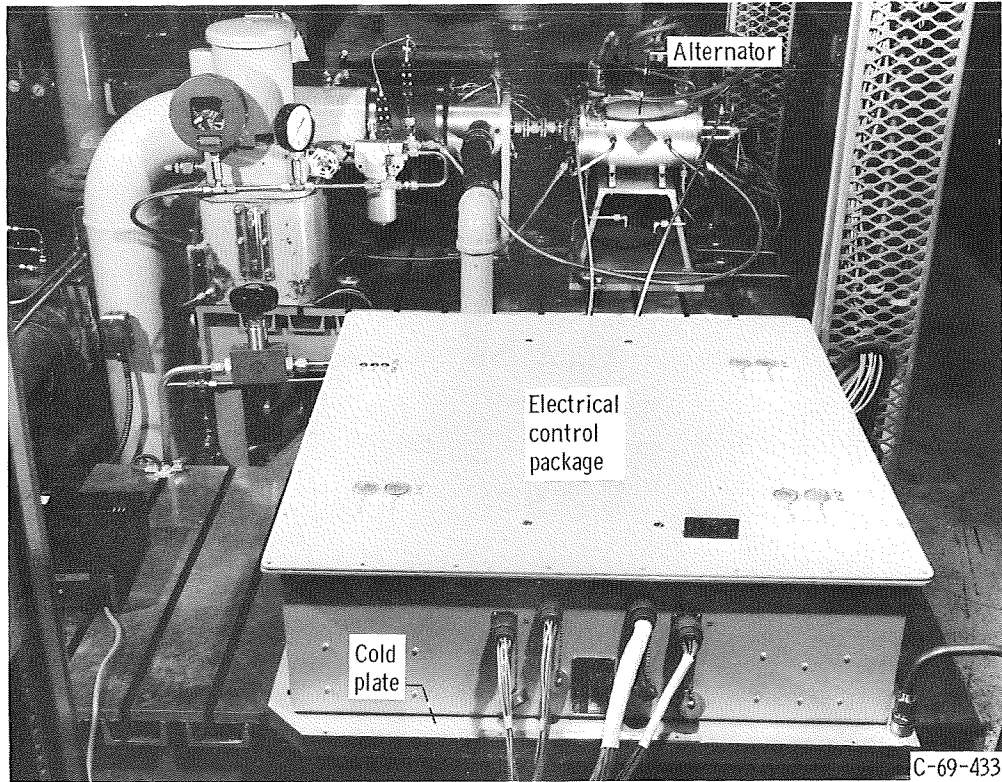
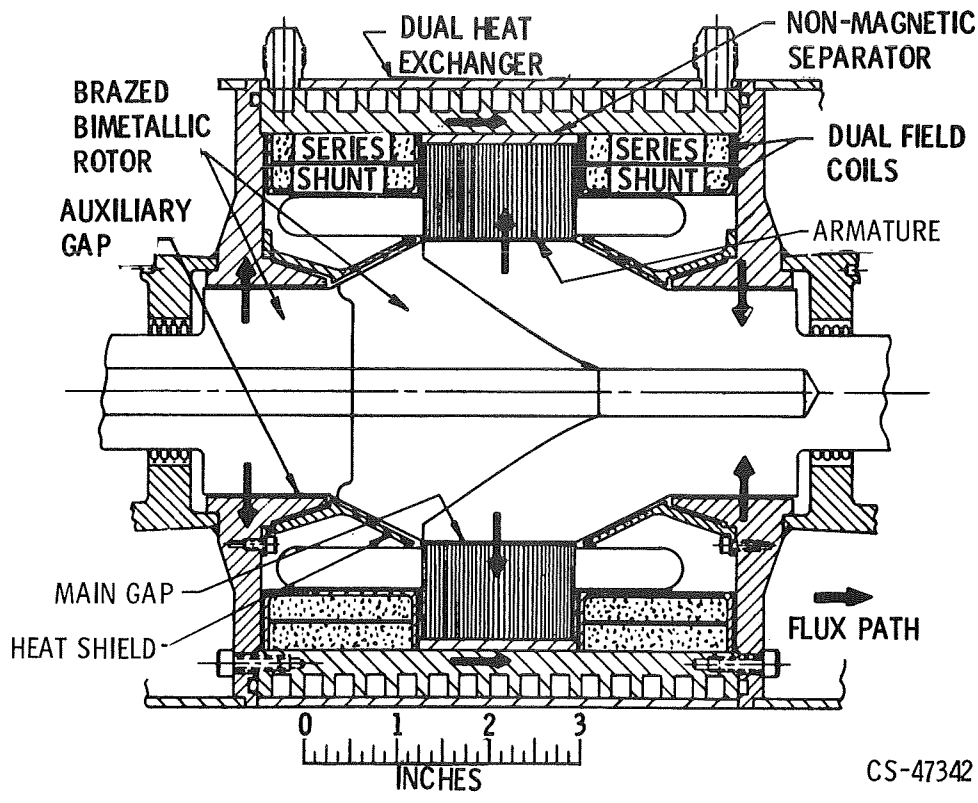


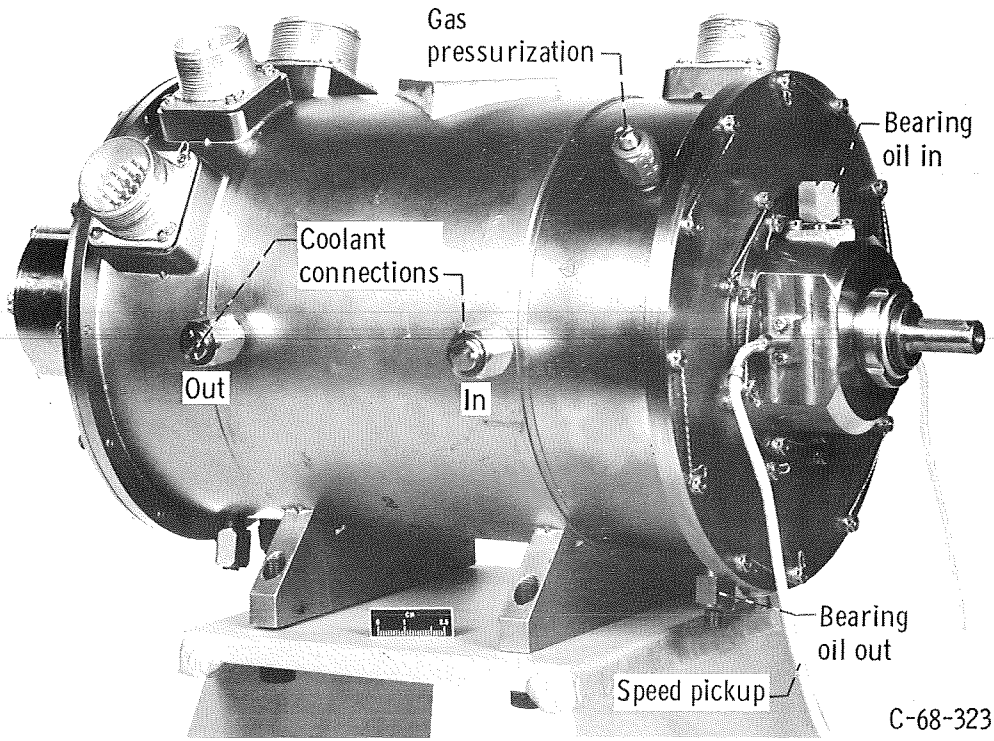
Figure 2.

E-5626



CS-47342

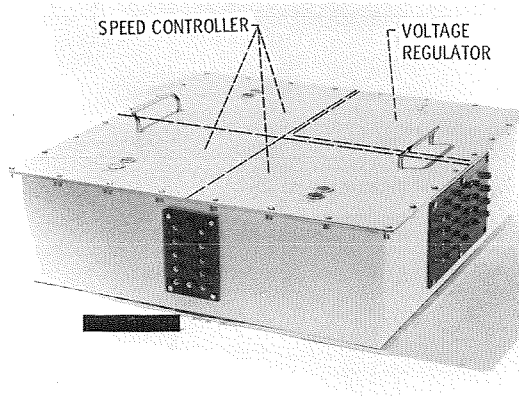
(a) Sectional view.



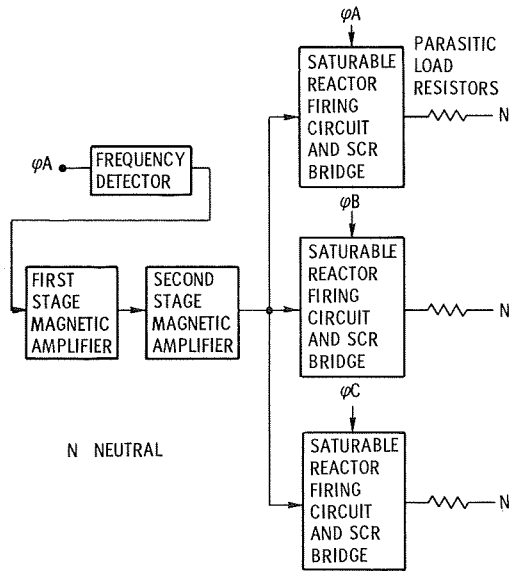
C-68-323

(b) Research alternator.

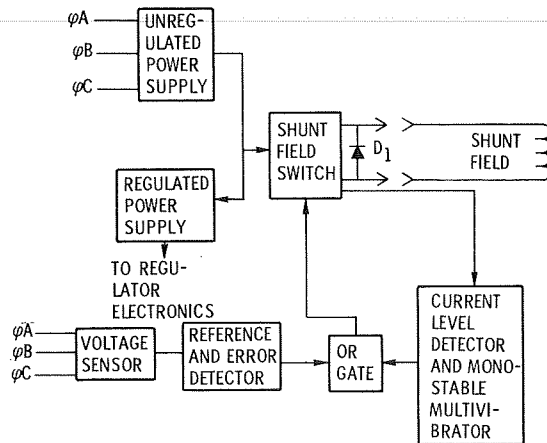
Figure 3.



(a)



(b) Block diagram of speed control (1 channel).



(c) Block diagram of shunt field regulator.

Figure 4. - Electrical control package.

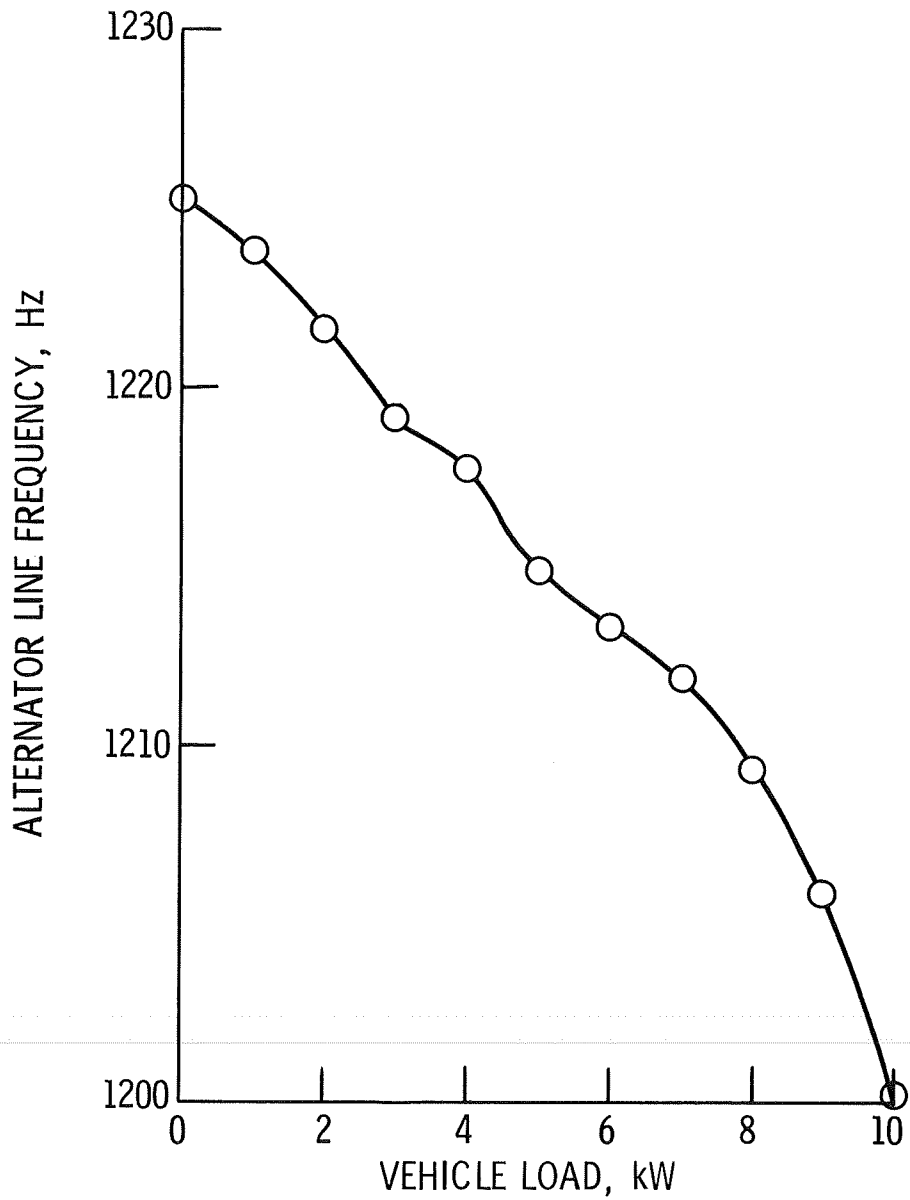


Figure 5. - Alternator frequency against vehicle load for 10.7 kW total alternator output at 0.85 vehicle load power factor lagging.

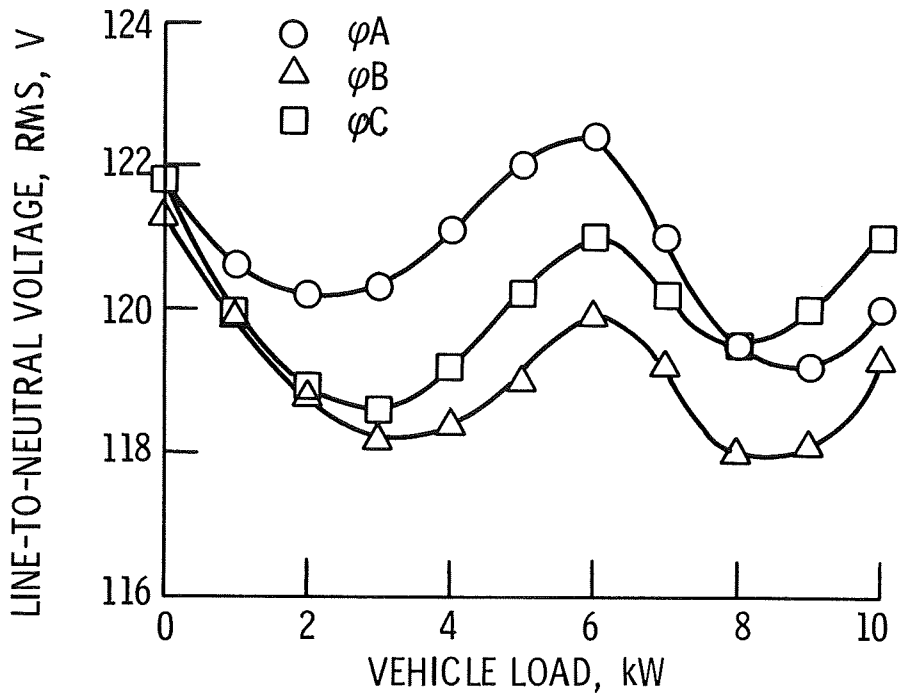


Figure 6. - Vehicle load voltages against vehicle loads for 10.7 kW total alternator output and 0.85 vehicle load power factor lagging.

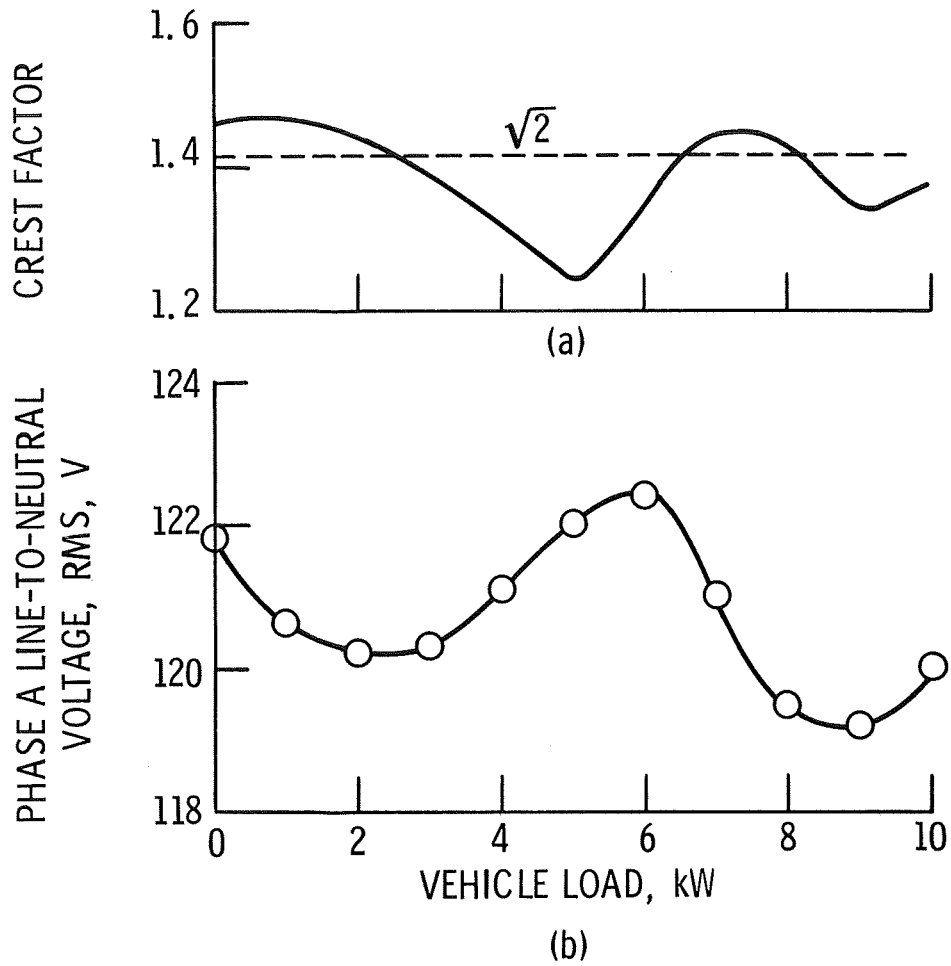


Figure 7. - Inter-relation of crest factor and phase A line voltage for vehicle loads at 0.85 power factor with 10.7 kW total alternator load.

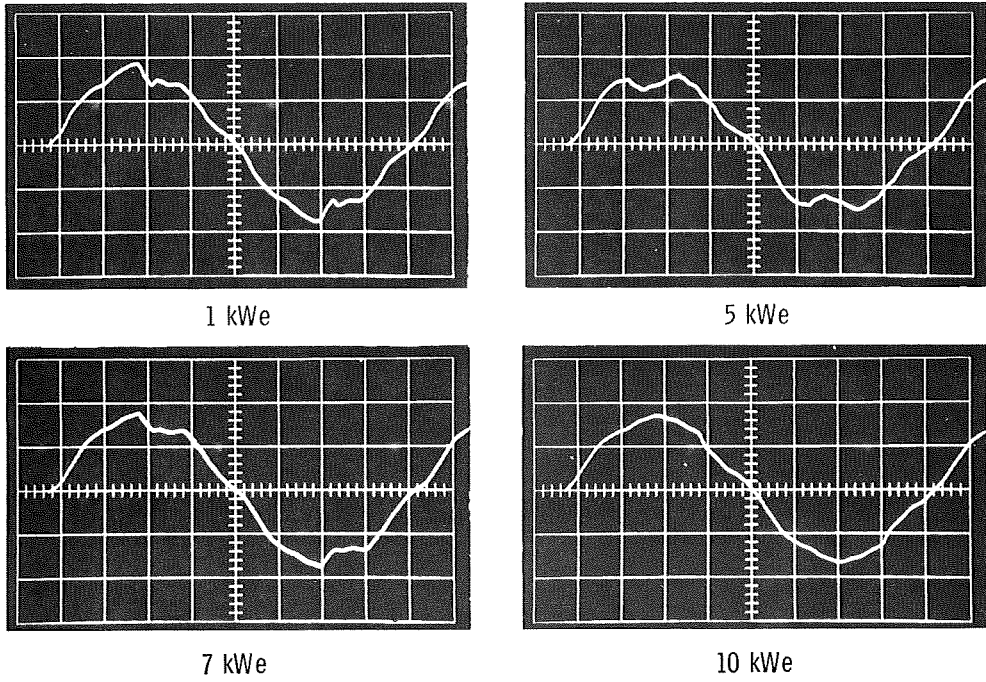
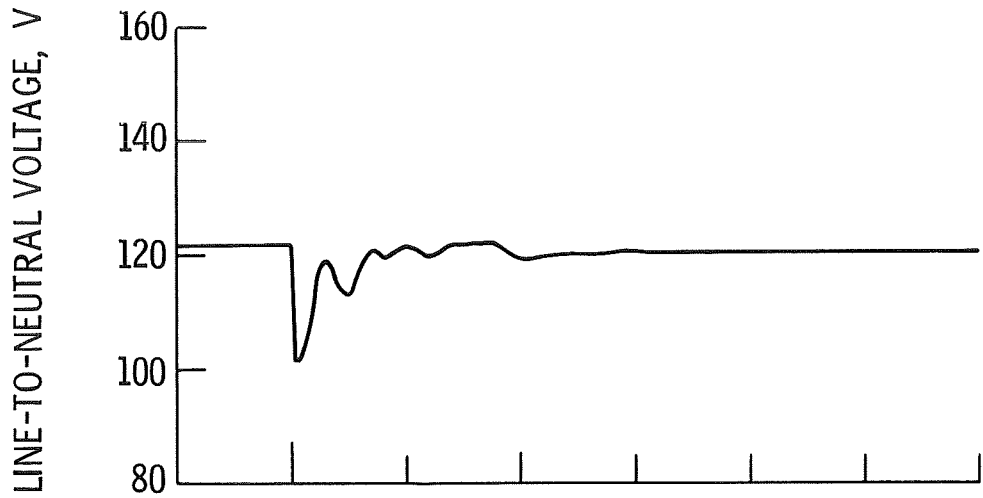
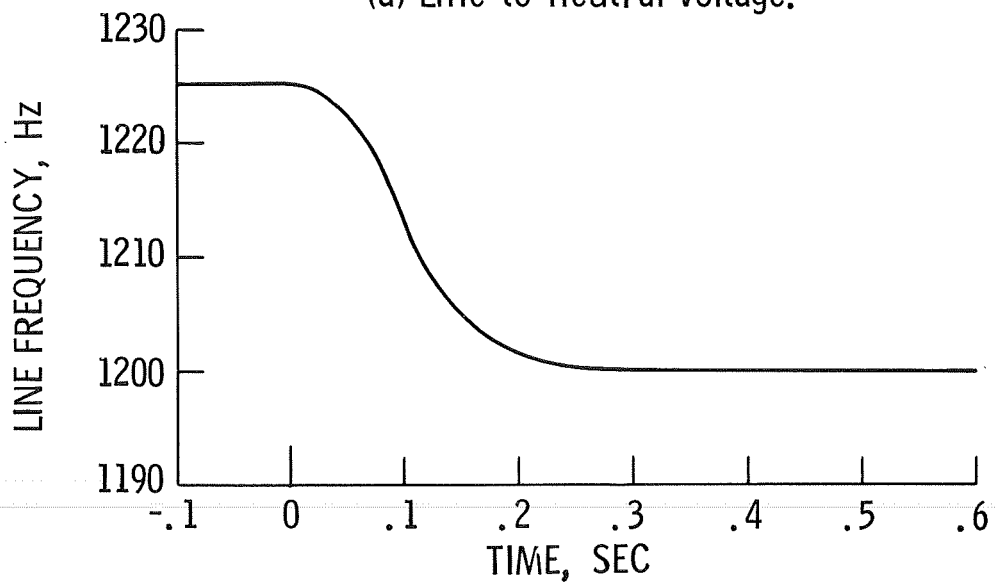


Figure 8. - Phase A vehicle load voltage for vehicle loads of 1, 5, 7, and 10 kW at 0.85 PF.

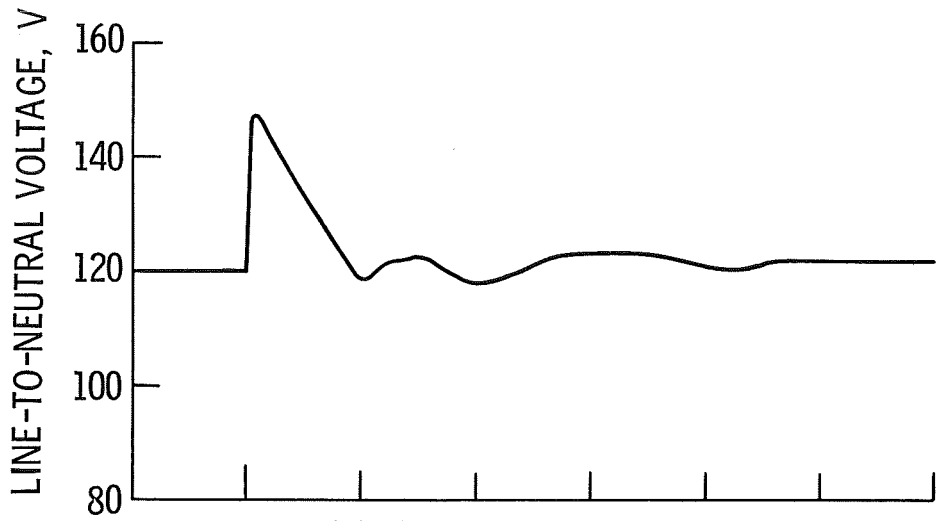


(a) Line-to-neutral voltage.

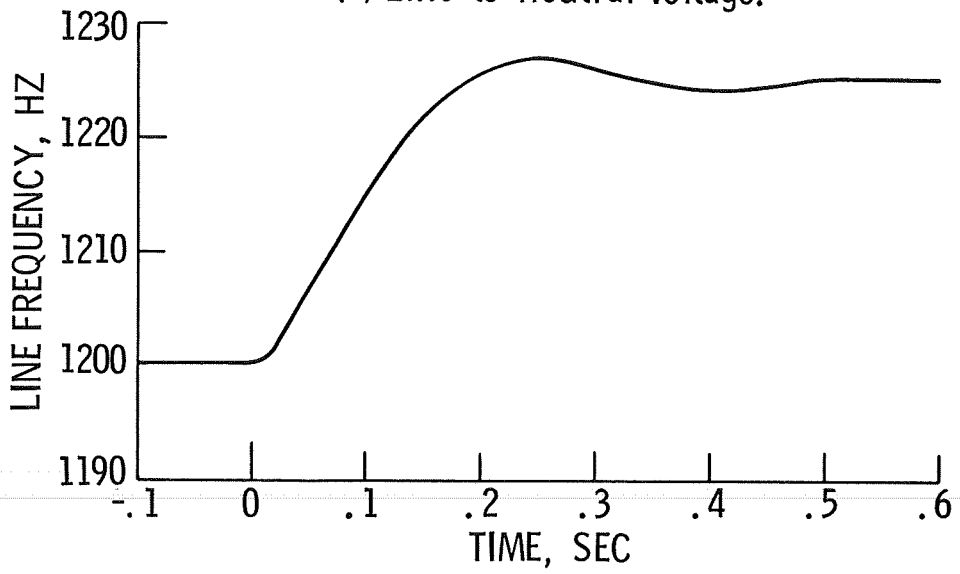


(b) Alternator line frequency.

Figure 9. - Response to a step application of 10 kW, 0.85 power factor (lagging) vehicle load.

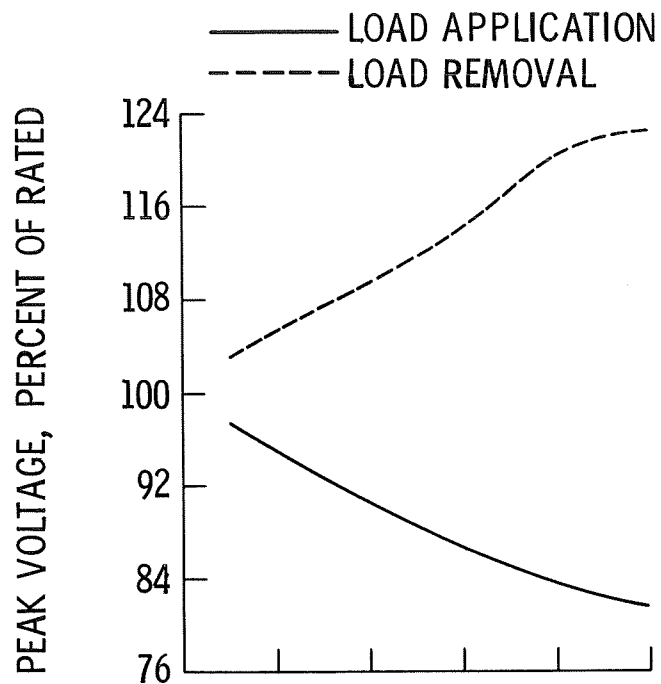


(a) Line-to-neutral voltage.

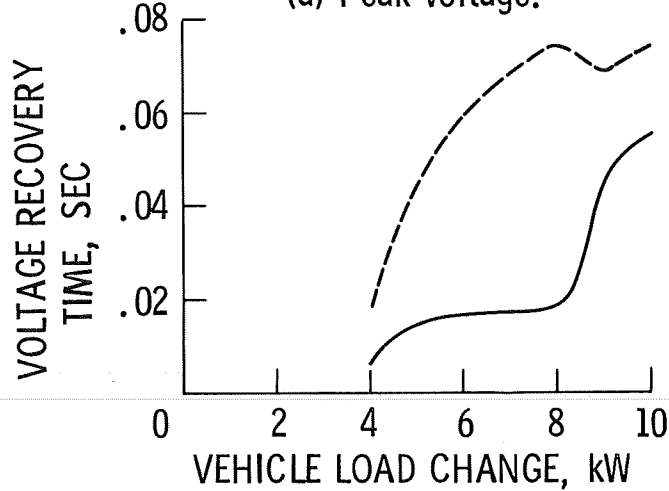


(b) Alternator line frequency.

Figure 10. - Response to a step removal of 10 kW, 0.85 power factor (lagging) vehicle load.

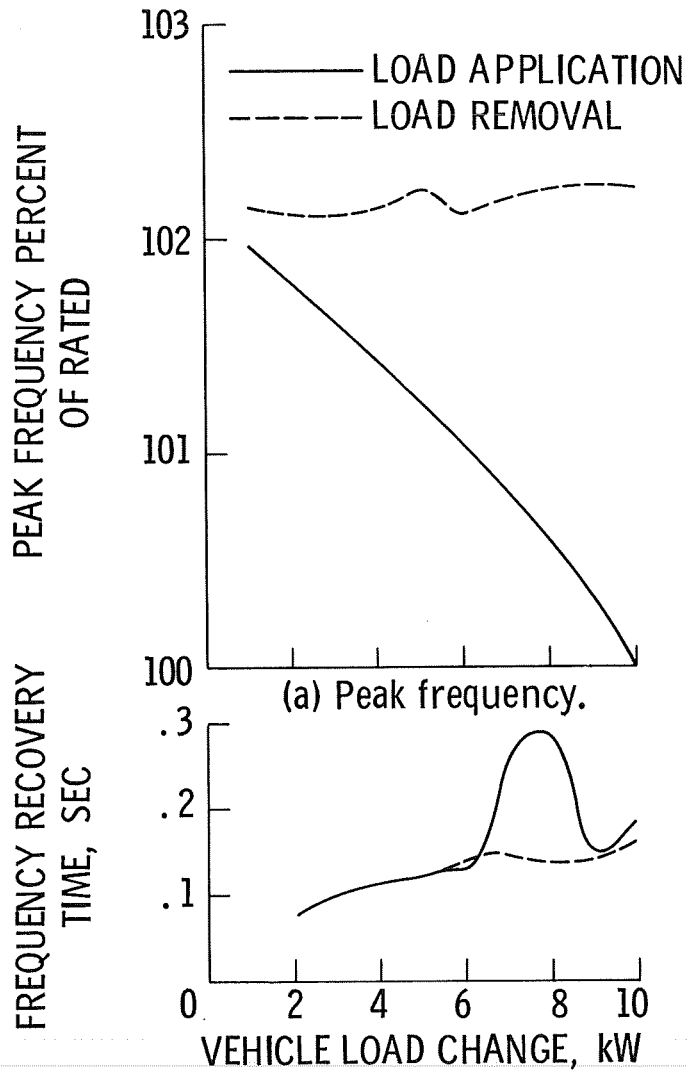


(a) Peak voltage.



(b) Recovery time.

Figure 11. - Voltage characteristics for step vehicle load changes at 0.85 power factor.



(b) Recovery time.

Figure 12. - Frequency characteristics for step vehicle load changes at 0.85 power factor.